Design of Multifunctional Honeycomb Materials

Carolyn Conner Seepersad,* Benjamin M. Dempsey,* Janet K. Allen,† Farrokh Mistree,‡ and David L. McDowell§
Georgia Institute of Technology, Atlanta, Georgia 30332-0405

Extruded metal honeycombs [linear cellular alloys (LCAs)] are designed for a multifunctional application that demands not only structural performance but also heat transfer capabilities. The manufacturing process for LCAs enables complex in-plane cell topologies that may be tailored to achieve desired functionality. As a result, certain mechanical and heat transfer properties of LCAs are superior to those of hexagonal honeycombs or stochastic metal foams. Both periodic and functionally graded LCAs are designed for a structural heat transfer device for an electronic cooling application. The design problem is formulated as a multiobjective decision. Approximate models of structural and heat transfer performance, such as finite difference heat transfer simulations, are employed to analyze designs efficiently. A portfolio of heat exchanger designs is generated with both periodic and functionally graded cell topologies. Tradeoffs are assessed between thermal and structural performance. Previous authors have focused primarily on analysis of the structural and thermal properties of cellular materials; here, a design perspective is adopted. Given a set of rigorous analytical models, the emphasis is on synthesis of cellular designs and identification of superior design regions.

Nomenclature

A	=	coefficient matrix
$A_i(\boldsymbol{x})$	=	achievement of a goal
$\boldsymbol{b}$	=	applied load vector
c_p	=	specific heat of the fluid
$c_{p_{av}}$	=	specific heat evaluated at the mean of the inlet and exit temperature
D	=	heat exchanger depth
d_h	=	internal width of a cell
d_i^+	=	overachievement deviation variable
d_i^-	=	underachievement deviation variable
d_v	=	internal height of a cell
E_s	=	elastic modulus of solid material
$\tilde{E}_x$	=	overall structural elastic stiffness in x direction
$\tilde{E}_y$	=	overall structural elastic stiffness in y direction
G_i	=	goal target value
Gr	=	Grashof number
H	=	heat exchanger height
h_i	=	height of cells in row i
k_f	=	fluid conductivity
k_s	=	solid cell wall conductivity
L	=	total length of the linear cellular alloy (LCA)
$\dot{M}$	=	total mass flow rate
$\dot{m}$	=	mass flow rate per cell in an LCA with a uniform cross section
$\dot{m}_{cell}$	=	mass flow rate in a cell
N	=	total number of nodes
N_h	=	number of cells in horizontal direction
Nu	=	Nusselt number
N_v	=	number of cells in vertical direction
n	=	total number of cells in an LCA cross section
Q	=	total heat transfer rate
Re	=	Reynolds number
T_{exit}	=	exit fluid temperature of a cell
T_{in}	=	inlet temperature of the fluid
T_s	=	specified constant wall temperature
t_h	=	horizontal cell wall thickness
t_v	=	vertical cell wall thickness
W	=	heat exchanger width
W_i	=	weight for goal I
w_i	=	width of cells in column i
$\boldsymbol{x}$	=	unknown temperature vector
Z	=	deviation or objective function
Δl	=	nodal spacing in the z direction
ΔP	=	pressure drop
Δx	=	nodal spacing in the x direction
Δy	=	nodal spacing in the y direction
ρ_f	=	density of the fluid

*Graduate Research Assistant, G.W. Woodruff School of Mechanical Engineering. Member AIAA.
†Senior Research Scientist, G.W. Woodruff School of Mechanical Engineering. Senior Member AIAA.
‡Professor, G.W. Woodruff School of Mechanical Engineering; farrokh.mistree@me.gatech.edu. Associate Fellow AIAA.
§Regents' Professor and Carter N. Paden, Jr., Distinguished Chair in Metals Processing, G.W. Woodruff School of Mechanical Engineering.

I. Introduction

MULTIFUNCTIONAL materials are integrated systems that serve multiple roles such as structural load bearing, thermal management, energy absorption, or other roles. These multifunctional material systems have compelling potential applications, including actively cooled supersonic aircraft or spacecraft skins, engine combustor liners, and lightweight structural elements with internal damping. Linear or two-dimensional cellular materials are particularly suitable for multifunctional applications that require not only structural performance but also lightweight thermal or energy absorption capabilities. Certain structural and thermal properties of extruded cellular honeycomb materials, so-called linear cellular alloys (LCAs), are superior to those of metallic foams with equivalent densities. For example, LCAs exhibit greater in-plane stiffness and strength and out-of-plane specific energy absorption than stochastic metal foams.[1,2] LCAs are advantageous as heat exchangers due to larger surface area density and lower pressure drop, two factors that compensate for lower heat transfer coefficients for laminar forced convection than for turbulent forced convection in stochastic metal foams with comparable relative densities.[3]

In addition, the manufacturing process for LCAs facilitates the fabrication of multifunctional cellular materials. Powder slurries are extruded through a die and then exposed to thermal and chemical treatments in a process developed by the Lightweight Structures Group at the Georgia Institute of Technology.[4] Extruded metallic cellular structures can be produced with nearly arbitrary two-dimensional cellular topologies limited only by paste flow and die manufacturability. Wall thicknesses and cell diameters as small

as fifty and several hundred micrometers, respectively, have been manufactured.[5]

Several authors have reported multifunctional analyses of two-dimensional cellular materials. Torquato et al.[6] establish cross-property bounds on the thermal conductivities of periodic hexagonal, triangular, and square cells in terms of elastic properties and vice versa. Gu et al.[7] present analytical models and dimensionless indices that enable simultaneous evaluation of structural and heat transfer performance of periodic hexagonal, square, and triangular cells. Structural performance is measured in terms of the effective shear modulus, whereas a corrugated wall model[3] is recommended for heat transfer. The nondimensional indices include a thermal performance index, calculated as the ratio of total heat transfer rate to pressure drop, and a thermomechanical index formulated by multiplication of the thermal index by the ratio of shear modulus to the modulus of elasticity of the solid material. Both Gu et al.[7] and Evans et al.[1] employ the indices to evaluate the performance of periodic triangular, square, and hexagonal topologies for thermomechanical applications. Hayes et al.[2] use theoretical estimates and physical experiments to evaluate several thermal and mechanical characteristics of LCAs, including total heat transfer rate; elastic properties; initial plastic buckling strengths; and in-plane and out-of-plane compressive strength, collapse behavior, and energy absorption for both quasi-static and dynamic loading. The steady-state heat transfer rate is evaluated for periodic square cells by the use of a finite difference approach that is more rigorous than closed-form estimates because it accounts for three-dimensional temperature distribution throughout the LCA and the convective fluid. The finite difference approach can accommodate functionally graded cell topologies, although Hayes et al. did not leverage this capability.

In this paper, we design multifunctional, two-dimensional cellular structures for applications that require both structural and thermal performance. Whereas previous authors have focused primarily on analysis of the structural and thermal properties of cellular materials, we adopt a design perspective; given a set of rigorous analytical models, our emphasis is on synthesis of cellular designs and identification of superior design regions. In the next section, we outline the boundary conditions and objectives for a structural heat exchanger for an electronic cooling application. Models are presented for evaluation of the required thermal and mechanical properties of the device. Like Hayes et al.,[2] we use a finite difference approach to evaluate steady-state heat transfer. At present, we consider only rectangular cell topologies, but as a noteworthy contribution, the analysis accommodates functionally graded dimensions and is not limited to periodic cells. A multiobjective decision support model, the compromise decision support problem (DSP), is presented for structuring the search for satisfactory multifunctional designs. In Sec. III, the compromise DSP and the proposed analytical models are used to synthesize LCA-based structural heat exchangers.

II. Design and Analysis Approach

LCAs are potentially well suited for heat exchanger applications, including compact electronic cooling devices and ultralight, actively cooled, aerospace structures. Unlike most heat exchangers, however, the two-dimensional cells that dissipate heat via conduction and convection also have desirable structural properties. Our goal for the present example is to determine appropriate cell shapes and sizes to achieve desirable values for two objectives: 1) overall rate of steady-state heat transfer and 2) overall structural elastic stiffness of the structure.

The device shown in Fig. 1 is a sample compact heat exchanger for a representative electronic cooling application in which the device is required to dissipate heat and support structural loads. The device has fixed overall width W, depth D, and height H of 25, 75, and 25 mm, respectively. It is insulated on the left, right, and bottom sides and is subjected to a heat source at constant temperature T_s on the top face. The mechanism for heat dissipation is forced convection via air with entry temperature T_{in} and total mass flow rate $\dot{M}$. The flow rate is variable, but it is linked to the available pressure head through a representative characteristic fan curve (Fig. 2). Steady-state, incompressible laminar flow is assumed. The solid material in
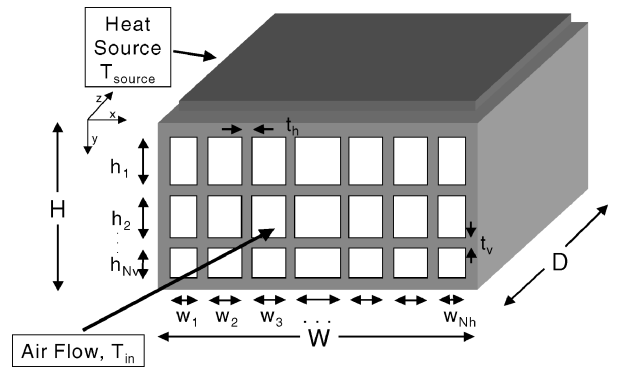

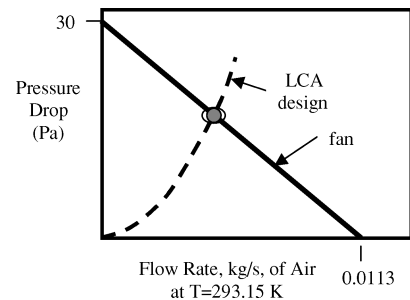Fig. 1   Compact, forced convection heat exchanger with graded rectangular LCAs.

Fig. 2   Characteristic fan curve.

the device is copper. The thermal conductivity k_s of copper samples fabricated with the thermochemical LCA extrusion process has been measured to be 363 W/m · K (Ref. 5).

For this example, the LCA is composed exclusively of rectangular cells, but the size, shape, and number of cells are permitted to vary in a graded manner. Each row of cells may assume a different height h_i and each column a different width w_i. The only restriction on cell height and width is that the cells must fit within the external dimensions with sufficient remaining space for vertical cell walls of variable thickness t_h and horizontal walls of variable thickness t_v. The numbers of cells in the horizontal and vertical directions are designated N_h and N_v, respectively.

To determine appropriate cell numbers and dimensions with the aim of maximizing both total heat transfer rate and overall structural elastic stiffness, it is necessary to formulate and solve a multiobjective decision. Our template for multi-objective decision making, the compromise DSP, is reviewed in Sec. II.D. For this example, informed multi-objective decision making requires thermal and structural analyses of the proposed design; our techniques are reviewed presently.

A. Finite Difference Heat Transfer Analysis of LCAs

The finite difference method is a numerical technique for solving the three-dimensional steady-state heat transfer equations—Fourier's law (conduction), Newton's law of cooling (convection), and an energy conservation for the internal flow—associated with the sample LCA heat exchanger shown in Fig. 1 (Ref. 8). The thermal system is subdivided into a number of small solid and fluid elements and associated nodes. The three-dimensional steady-state heat transfer equations are solved numerically for the mesh via a central difference method with second-order accuracy. The finite difference method is used in this example to approximate the temperature distribution in an LCA heat exchanger and the total rate of steady-state heat transfer from the LCA to the fluid flowing through the cells. The thermal boundary conditions for the LCA heat exchanger in Fig. 1 include a heated top surface with fixed temperature. The left, right, and bottom sides are insulated, and the entry and exit surfaces are exposed to convective flow. Because the ratio of the Grashof number Gr to the squared Reynolds number Re^2 is
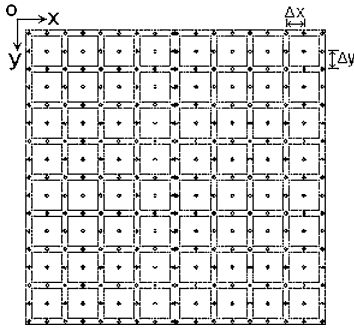
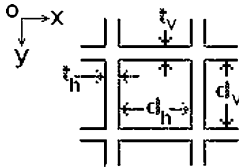**Fig. 3   Finite difference nodal placement on a typical cross section of LCA.**

Fig. 4   Single cell with related dimensions.

much less than unity for the conditions considered in this example, natural convection is neglected.[8]

With the finite difference method, an LCA is discretized by nodes located distances Δx and Δy apart within each cross section of the LCA (Fig. 3). The cross sections are located a distance of Δl apart along the length of the LCA in the z direction in Fig. 1. Nodal spacing Δl is chosen via grid convergence. The spacing Δx is specified as the distance between nodes in the x direction, that is, $\Delta x = (t_h + d_h)/2$, where t_h and d_h are the horizontal cell wall thickness and internal cell width, respectively (Fig. 4). The spacing for Δy is found in a similar manner. The spacing is dictated by cell size because the internal cell dimensions d_h and d_v can vary in a given cross section. Because Δx and Δy are based on d_h and d_v, these variables can have a range of values within a given cross section. The fluid contained within each cell over a length Δl (control volume element) is assigned a uniform temperature. This is an approximation that provides a first-order solution to the three-dimensional steady-state heat transfer problem and promotes solution efficiency.

When the steady-state three-dimensional heat transfer equations are expressed in a finite difference formulation, assumptions are made to facilitate efficient solution. A relatively coarse set of finite difference nodes are employed in this work. This places limitations on the accuracy and fidelity of temperature gradients to increase solution efficiency. Cell walls are composed of a metal alloy with conductivity k_s assumed constant over the range of temperatures evaluated. Temperature is assumed constant in cell wall segments surrounding each finite difference node, as well as in the fluid within each incremental length of a cell. The fluid properties, including specific heat c_p, conductivity k_f, and density ρ_f, are evaluated at the mean fluid temperature of the inlet and exit.[8] The functions used to evaluate the fluid properties, except specific heat, are curve fits to tabulated data.[8] The specific heat is found with a standard equation.[9] The inlet fluid temperature T_{in} is assumed constant over the entire cross section. The pressure drop is assumed to follow from laminar flow tabulations for rectangular ducts.[10]

Based on the finite difference approach and the preceding assumptions, a linear system of equations is constructed by evaluation of the energy balance for each node in the LCA. This system of equations can be expressed in matrix notation as[11]

$$Ax = b \qquad (1)$$

A is the coefficient matrix, b is the applied load vector, and x is the unknown temperature vector. The goal is to solve for the unknown temperature vector x. The fluid elements interact with the surrounding walls and the fluid element one increment Δl upstream in the flow. Hence, the A matrix is unsymmetric, and the solution must be obtained with an unsymmetric solver. Each node interacts with 10 surrounding nodes. Six of these nodes are $\pm \Delta x$, $\pm \Delta y$, or $\pm \Delta l$ in the x, y, and z directions. The remaining four interacting

nodes are neighboring diagonal nodes. This creates a sparsely populated, banded matrix. Because each row of the A matrix can have a maximum of 11 nonzero values (one for each direction and one for the node itself), solution storage requires only two $N \times 11$ matrices, where N is the number of nodes. All of the nonzero values are stored in one matrix, and the locations of these values in the overall expanded A matrix are stored in the other matrix. A technique for efficiently storing a large, sparsely populated matrix in the context of an lower–upper (LU) decomposition was described by George.[12] A similar technique is used in this work to reduce the total number of stored values in the coefficient matrix from N^2 to $22 \times N$. A successive overrelaxation method[13] can be used to solve a single A matrix, and this standard method has been extended in this work to solve two matrices and determine the temperature distribution throughout the LCA structure. Once the exit temperatures of the fluid in each cell are found, the total rate of steady-state heat transfer is calculated[8] by a summation over all of the cells, that is,

$$Q = \sum_i^{n\,\text{cells}} \dot{m}_{\text{cell}_i} c_{p_{\text{av}}} \left(T_{\text{exit}_i} - T_{\text{in}} \right) \qquad (2)$$

where $\dot{m}_{\text{cell}}$ is the mass flow rate of a cell, $c_{p_{\text{av}}}$ is the specific heat of the fluid evaluated at the mean temperature of the fluid, T_{exit} is the fluid exit temperature of a cell, and T_{in} is the inlet temperature of the fluid.

B.   Validation of Finite Difference Code

The accuracy of the finite difference code is validated by comparison with 1) physical experiments, 2) an isothermal analytical solution, and 3) a computational fluid dynamics code. In Figs. 5 and 6, finite difference based predictions of total rates of steady-state heat transfer are plotted along with data from physical experiments for $Re = 1200$ and 891 for room temperature air entering the cells
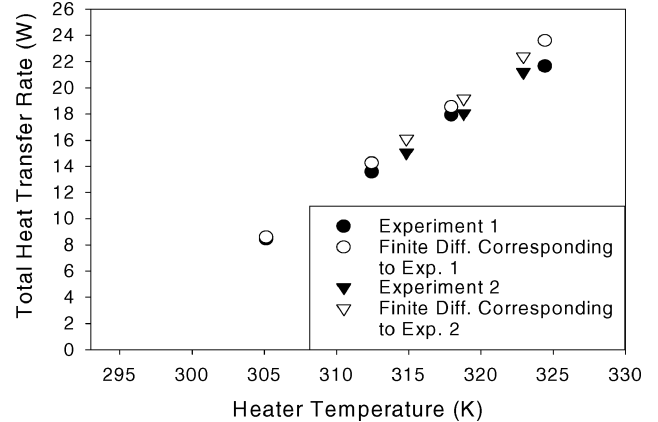

Fig. 5   Comparison of experimental results with finite difference predicted values for $Re = 1200$.
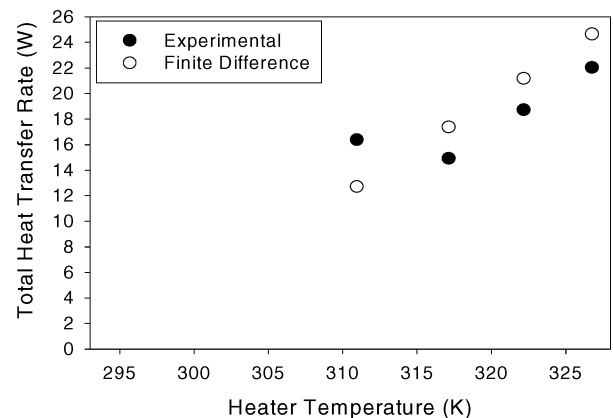

Fig. 6   Comparison of experimental results with finite difference predicted values for $Re = 891$.

of an LCA. The cells are square with 0.16-cm inner dimensions, and they are arranged in eight rows and eight columns within an LCA of overall width, height, and length of 1.38, 1.38, and 5.08 cm, respectively. Boundary conditions, cellular material configuration, and dimensions are equivalent for the physical experiment and the finite difference analysis. Additional details are provided by Dempsey.[14] There is a strong correlation between the experimental results and the predicted values of the total rate of steady-state heat transfer; thus, we conclude that the finite difference code reasonably predicts the observed behavior of LCAs as heat exchange devices in the laminar flow regime.

Analytical calculations for isothermal cell walls are used to obtain a theoretical upper bound for the rate of steady-state heat transfer that can be compared with finite difference based estimates for equivalent conditions. If the cell walls are assumed to be perfect conductors with constant temperature T_s, the theoretically maximum rate of heat transfer for each LCA cell is expressed by the relation[15]

$$Q = \dot{m} c_p (T_s - T_{\text{in}}) \left[1 - \exp\left(\frac{-4NuLk_f}{\dot{m} c_p} \right) \right] \qquad (3)$$

where Q is the total heat transfer into a cell, c_p is the specific heat, T_{in} is the mean inlet fluid temperature, L is the length of the LCA, and $\dot{m}$ is the mass flow rate per cell. For comparison purposes, isothermal cell wall conditions are approximated in the finite difference analysis by assignment of very large solid conductivity values (1×10^{21} W/m · K) for the cell walls. Several parameters are assigned equivalent values in the finite difference and theoretical isothermal analysis, including the inlet fluid temperature of 273 K, the total mass flow rate of 0.0005 kg/s, the heated wall temperature of 373 K, and the external dimensions of the LCA in the x, y, and z directions of 12.5, 20, and 25 mm. A range of square cell dimensions from 0.5 to 3 mm are examined, such that the mass flow rate per cell and the number of cells per cross section vary. For the range of cell sizes, the corresponding average velocity per cell ranges from 3.01 to 2.42 m/s with Reynolds numbers from 84 to 471. The isothermal solution and the finite difference approximation are compared for these conditions, and the maximum error between finite difference estimates and theoretical isothermal calculations for total rates of steady-state heat transfer is less than 6% over the range of square cell dimensions. Similar findings apply for higher mass flow rates and corresponding Reynolds numbers.

The experiments and the isothermal solution pertain to uniform arrays of square cells, but it is also possible to fabricate graded cell structures with this technology. To validate the finite difference code in the context of graded structures, the computational fluid dynamics software FLUENT[16] is employed. An LCA is analyzed with constant overall mass flow rate of 0.0005 kg/s, uniform inlet fluid temperature of 293.15 K, and external dimensions in the x, y, and z directions of 9, 17.4, and 25 mm, respectively. This overall mass flow rate results in a maximum cell fluid velocity of 2.0×10^{-5} m/s and a maximum Reynolds number of 727 for this configuration. Three of the external walls are adiabatic, and the top wall is held at a constant temperature (393.15 K). There are four uniform cell columns (2-mm width each) and three graded cell rows (10-, 5-, and 2-mm heights) with the largest cells near the heat source. The wall thicknesses in the x and y directions are constant (0.2 and 0.1 mm, respectively). For nonuniform cell sizes, it is necessary to solve the linear momentum and continuity equations simultaneously in the finite difference code to partition the mass flow rate among cells, under the assumption that the cells are infinitely long compared to their diameters. This is a first-order approximation in the finite difference approach, whereas FLUENT accounts for details of the fluid entry effects. The grid in FLUENT is refined to fluid elements with dimensions $0.5 \times 0.5 \times 0.625$ mm with two elements through the wall thickness. The cellular structure is analyzed for the specified conditions by the use of both FLUENT and the finite difference code on a single 450-MHz Intel Pentium II processor with 512 MB of RAM. Total rates of steady-state heat transfer derived from a fully converged FLUENT solution are approximately 10% greater than the finite difference estimates. For a comparison of convergence speeds, a FLUENT model is created with a coarser mesh and with prediction accuracy equivalent to finite difference code capabilities. A FLUENT analysis with the coarser mesh requires 7.2 min to converge to within 10% of the finite difference solution for the representative case described earlier. In contrast, the finite difference code provides a solution for the same analysis in 1.2 s. The time required for a single analysis is significant given that a search/optimization algorithm requires tens and typically hundreds of analyses to identify each of the preferred designs reported in Sec. III. By comparing the finite difference analysis with FLUENT, we conclude that the finite difference code yields approximate solutions quickly and with sufficient accuracy to explore the design space.

C. Theoretical Estimates of Structural Properties

The structural performance of an LCA heat exchanger is evaluated in terms of the overall structural elastic stiffness of the structures. Several authors have reported effective elastic moduli for two-dimensional cellular materials with periodic hexagonal, square, or triangular topologies.[6,7,17] Hayes et al.[2] also report elastic properties for other cell shapes, including periodic rectangular cells. These analytical estimates are not appropriate, however, for the nonperiodic rectangular cell structures explored in this example.

When an LCA with nonperiodic rectangular cells is loaded along one of the coordinate axes in Fig. 3, elastic deformation occurs due to axial extension or compression of the cell walls. If the loading is axial, and there are no imperfections in the structure, there is no bending contribution to the deformation in this particular loading configuration. Thus, the overall structural elastic stiffness in the x direction, $\tilde{E}_x$, or y direction, $\tilde{E}_y$, is approximated as the fraction of the total width W or height H, respectively, occupied by cell walls, that is,

$$\tilde{E}_x / E_s \cong [t_h (N_H + 1)] / W \qquad (4)$$

$$\tilde{E}_y / E_s \cong [t_v (N_V + 1)] / H \qquad (5)$$

where E_s is the elastic modulus of the isotropic solid cell wall material. As a lower bound on the overall structural elastic stiffnesses, the expressions for effective elastic stiffnesses of a periodic array of rectangular cells[2] are employed, with w and h replaced by the largest cell width and the largest cell height, respectively, that is,

$$E_x / E_s = t_v / h \qquad (6)$$

$$E_y / E_s = t_h / w \qquad (7)$$

By the use of these expressions, structural capability can be assessed in addition to thermal performance.

D. Multiobjective Decisions

Design of cellular materials is a synthesis activity. It is structured via formal decision models that facilitate exploration of a multifunctional design space with the assistance of domain-specific models such as the thermal and structural analysis approaches described earlier. Our approach for supporting multiobjective decision making is through the use of the compromise DSP, a generic multi-objective decision model.[18] The compromise DSP is a mathematical construct that is used to determine the values of design variables that satisfy a set of constraints and achieve as closely as possible a set of conflicting goals. A compromise DSP is stated in words as follows:

Given	Relevant information
Find	The values of the independent system variables, and the values of the deviation variables (which indicate the extent to which goals are achieved)
Satisfy	System constraints that must be satisfied for the solution to be feasible, bounds on the system variables, and goal constraints
Minimize	The deviation of the system performance from established goals

The mathematical form of a compromise DSP is summarized in Fig. 7. The system descriptors, namely, system and deviation variables, system constraints, system goals, bounds, and the deviation

Given
An alternative to be improved through modification
Assumptions used to model the domain of interest
The system parameters:

	n	number of system variables
	$p+q$	number of system constraints
	p	equality constraints
	q	inequality constraints
	m	number of system goals

$C_i(\mathbf{x})$ Capability of the system

$D_i(\mathbf{x})$ Demand to the system

$g_i(\mathbf{x})$ System constraint function

$$g_i(\mathbf{x}) = C_i(\mathbf{x}) - D_i(\mathbf{x})$$

Find

X_i System Variables $i = 1, ..., n$

d_i^+, d_i^- Deviation Variables $i = 1, ..., m$

Satisfy
System Constraints (linear, nonlinear)

$$g_i(\mathbf{x}) = 0 \qquad i = 1, ..., p$$

$$g_i(\mathbf{x}) \geq 0 \qquad i = p+1, ..., p+q$$

System Goals (linear, nonlinear)

$$A_i(\mathbf{x}) + d_i^- - d_i^+ = G_i \qquad i = 1, ..., m$$

Bounds

$$X_{i,min} \leq X_i \leq X_{i,max} \qquad i = 1, ..., n$$

$$d_i^+, d_i^- \geq 0 \qquad i = 1, ..., m$$

$$d_i^+ \cdot d_i^- = 0 \qquad i = 1, ..., m$$

Minimize
Deviation Function: Archimedean formulation

$$Z = \sum_i W_i\left(d_i^+, d_i^-\right) \qquad i = 1, ..., m$$

Fig. 7   Mathematical formulation of the compromise DSP.[18]

function are described in detail elsewhere.[18] The compromise DSP is a hybrid formulation that incorporates concepts from both traditional mathematical programming and goal programming. The compromise DSP and mathematical programming are similar to the extent that they refer to system constraints that must be satisfied for feasibility. They differ in the way the deviation or objective function is modeled. In the compromise DSP, as in goal programming, multiple objectives are formulated as system goals involving deviation variables that measure the extent to which each goal is achieved, and the deviation function is modeled by the use of deviation variables rather than system or decision variables. The compromise DSP differs from goal programming, however, because it is tailored to handle common engineering design situations in which physical limitations are manifested as system constraints (mostly inequalities) and bounds on the system variables.

The conceptual basis of the compromise DSP is to minimize the difference between that which is desired (the goal G_i) and that which can be achieved [$A_i(x)$] for multiple goals. This is accomplished by minimization of the deviation function Z, expressed in terms of deviation variables. The deviation function provides a measure of the extent to which multiple goals are achieved. In the compromise DSP, multiple goals have been considered conventionally by formulation of the deviation function either with Archimedean weightings or preemptively (lexicographically).[18] In traditional mathematical programming, the objective function typically represents a single goal, by which the desirability of a design solution is measured. All other characteristics of a design are modeled as hard constraints. On the other hand, the compromise DSP is more flexible than traditional mathematical programming because it accommodates multiple constraints and objectives, as well as both quantitative information and information, such as bounds and assumptions, that may be based on a designer's judgment and experience.[19]

In the next section, the compromise DSP and thermal and structural analysis techniques are used to design multifunctional heat exchangers.

Table 1   Boundary conditions for design

Parameter	Value
Structure width W	0.025 m
Structure height H	0.025 m
Structure depth D	0.075 m
Inlet air temperature T_{in}	293.15 K
Heat source temperature T_{source}	373.15 K
Conductivity of solid material k	363 W/m·K
Total mass flowrate $\dot{M}$	Variable, tied to pressure drop via fan curve (Fig. 2)
Working fluid	Air

Given
Finite Difference Algorithm for Heat Transfer (Section 2.1)
Analytical Expressions for Overall Structural Elastic Stiffness (Section 2.3)
Boundary Conditions (Table 1)
Find
Phase 1: N_H, N_V, t_H, t_V, $\dot{M}$
Phase 2: t_H, t_V, $\dot{M}$, h_1, h_2, ..., h_{Nv}
Satisfy
Constraints:
Fan Curve (Figure 2): $\Delta P \leq 30 - (2663.35 * \dot{M})$
$Re \leq 2300$
System Goals:
All Phases:

$$\frac{Q_{total}}{Q_{total-target}} + d_1^- - d_1^+ = 1 \qquad \text{Eqn. 2}$$

Phase 2b:

$$\frac{\tilde{E}_x / E_s}{(\tilde{E}_x / E_s)_{target}} + d_2^- - d_2^+ = 1 \qquad \text{Eqn. 4}$$

$$\frac{\tilde{E}_y / E_s}{(\tilde{E}_y / E_s)_{target}} + d_3^- - d_3^+ = 1 \qquad \text{Eqn. 5}$$

Bounds on Design Variables:
Phase 1: $2 \leq N_H \leq 16$
         $2 \leq N_V \leq 16$
Phase 2:
     $0.00025 \text{ m} \leq h_i \leq 0.022 \text{ m}$
All Phases:
     $0.00015 \text{ m} \leq t_H \leq 0.002 \text{ m}$
     $0.00015 \text{ m} \leq t_V \leq 0.002 \text{ m}$
     $0.0005 \text{ kg/s} \leq \dot{M} \leq 0.003 \text{ kg/s}$

     $d_i^+, d_i^- \geq 0 \qquad d_i^+ \cdot d_i^- = 0$

Minimize

Phases 1 and 2a: $Z = W_1 d_1^-$

Phase 2b: $Z = W_1 d_1^- + W_2 d_2^- + W_3 d_3^-$
     ($W_1 = 0.5$, $W_2 = 0.25$, $W_3 = 0.25$)
($Q_{target} = 110$ W; $(\tilde{E}_x / E_s)_{target}$ and $(\tilde{E}_y / E_s)_{target}$ variable)

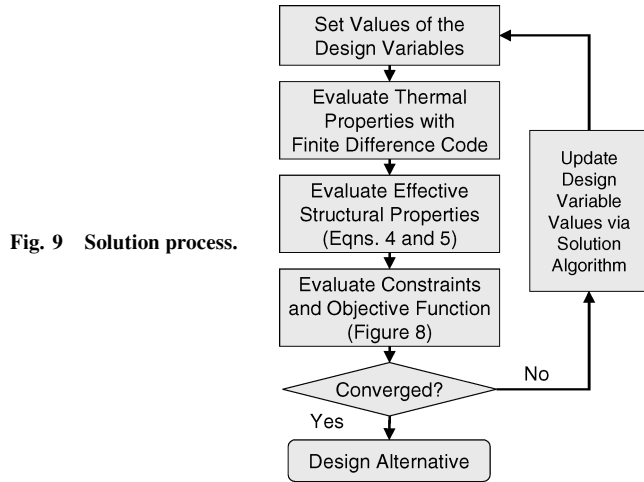**Fig. 8   Compromise DSP for heat exchanger.**

III.   Designing a Heat Exchanger for Electronic Cooling

Functionally graded LCA heat exchangers with desirable structural and thermal properties are designed for the boundary conditions listed in Table 1. Design is guided by using the compromise DSP in Fig. 8. Given a set of boundary conditions and analysis techniques for nonperiodic LCA heat exchangers, the objective is to find the values of design variables that satisfy constraints and bounds and achieve the targets for one or more goals as closely as possible. Design solutions are achieved by the use of iSIGHT[20] design automation and exploration software, coupled with the finite difference algorithms and analytical expressions described in Sec. II. The solution process is mapped in Fig. 9.

A two-phase design approach is employed, as outlined in Table 2. The two-phase approach facilitates management of design freedom, development of intuition with respect to desirable solutions, and exploration of the design space. In the first phase, preliminary layouts are explored for the cellular material in light of an established set of multifunctional requirements. This process could involve a

Table 2   Three-phase design approach

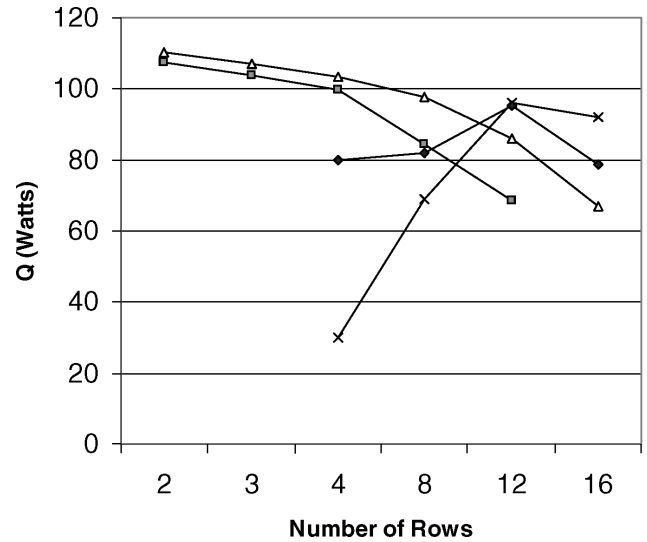| Phase	Design variables	Design objective(s)	Outcome
1	$N_H, N_V, t_H, t_V, \dot{M}$ (h and w are dependent variables)	Maximize Q_{total}	Determine the appropriate shape and number of cells.
2 part a	$t_H, t_V, \dot{M}, h_1, h_2, \ldots, h_{Nv}$ ($w_1, w_2, \ldots, w_{N_H}$ are uniform and dependent variables) (fix N_H and N_V)	Maximize Q_{total}	Determine functionally graded designs for number of cells determined in phase 1.
2 part b	$t_H, t_V, \dot{M}, h_1, h_2, \ldots, h_{Nv}$ ($w_1, w_2, \ldots, w_{N_H}$ are uniform and dependent variables) (fix N_H and N_V)	Maximize $Q_{\text{total}}, \tilde{E}_x/E_s, \tilde{E}_y/E_s$	Determine functionally graded designs that satisfy multiple objectives for number of cells determined in phase 1.

Fig. 9   Solution process.

Fig. 10   Total heat transfer rate of periodic rectangular cell LCAs with various numbers of rows and columns: ■, 16 columns; △, 12 columns; ✕, 4 columns; and ◆, 8 columns.

topology optimization technique or formal selection of a superior concept(s) from a finite set of feasible alternatives based on available quantitative and qualitative information. The outcome of this phase is a concept that embodies the basic geometry, arrangement, and topology of the material. In phase 2, the preliminary configuration identified in phase 1 is refined. Influential design variables, such as dimensions, are modified systematically to satisfy constraints and explore tradeoffs among a set of multifunctional objectives. The outcome of the second phase is a family or Pareto set of designs, based on a common concept, that embodies a range of multifunctional performance. Such a two-phase approach is particularly pragmatic when concepts with a broad range of shapes and sizes or fundamentally different cell configurations or topologies (such as standard square, triangular, or hexagonal cell shapes, or arbitrary shapes and arrangements obtained with topology optimization techniques) are identified, evaluated, and filtered in phase 1 and then refined for superior multifunctional performance in phase 2.

A.   Phase 1

In phase 1, the general layout of the cellular heat exchanger is determined, including the shape and approximate size of the cells. Because the primary objective is to maximize the rate of steady-state heat transfer for laminar flow within the cells, rectangular cell topologies are chosen; they exhibit higher Nusselt numbers than other standard topologies.[8] The layout of the material is characterized more completely by exploration and comparison of a range of feasible cell counts, sizes, and aspect ratios for superior steady-state heat transfer rates for the specified boundary conditions. As a preliminary exploration of the design space, the numbers of cells in the horizontal and vertical directions are varied, whereas the cells are assumed to be periodic with equivalent width and height. The thickness of the vertical cell walls t_h and the thickness of the horizontal cell walls t_v are also varied, along with total mass flow rate $\dot{M}$, which is tied to the pressure drop via the fan curve of Fig. 2. Two solution techniques may be used in phase 1: 1) exploratory solution algorithms such as simulated annealing and genetic algorithms that accommodate both discrete and continuous variables with $t_h, t_V, \dot{M}$, and N_H and N_V as design variables, or 2) gradient-based solution algorithms, such as sequential quadratic programming, that accommodate only continuous variables and must be employed repeatedly for fixed values of N_H and N_V, with t_h, t_V, and $\dot{M}$ as design variables. The latter approach is employed in this case. (Note that the strengths

and limitations of these two techniques are associated with the solution algorithms rather than the design approach itself.) All design solutions are validated carefully by employing multiple starting points for the solution algorithm, by reviewing trends and convergence in the data, and by monitoring active constraints and bounds.

An LCA structure with periodic, rectangular cells is designed for each combination of rows and columns depicted in Fig. 10. The ordinate axis in Fig. 10 represents maximum achievable total heat transfer rates for each configuration. As shown in Fig. 10, it is advantageous, from a thermal perspective, to employ 12 columns of cells and only a few rows of cells (2, 3, or 4). The 12 by 2, 12 by 3, and 12 by 4 configurations have the largest heat transfer rates and are investigated in phase 2. Designs with periodic rectangular cells for 12 by 2, 12 by 3, and 12 by 4 configurations are illustrated in Figs. 11a, 11d, and 11g. Note that these results may be sensitive to the stated boundary conditions and dimensions. Alternative numbers of rows and columns may be appropriate for other boundary conditions, dimensions, or cell shapes.

B.   Phase 2

In the second design phase, the preliminary layouts identified in phase 1 are refined to generate a family of designs with a broad range of multifunctional performance tradeoffs. Graded structures are designed to maximize a combination of the total rate of steady-state heat transfer, Q_{total}, and overall structural elastic stiffness in the x and y directions, $\tilde{E}_x/E_s$ and $\tilde{E}_y/E_s$, respectively. Specifically, graded cells are designed by permitting the height of each row of cells to vary independently. By the allocation of fractions of available height to each cell, rather than basic dimensions, we ensure that the sum of cell dimensions and wall thicknesses does not exceed the height of the structure. Wall thicknesses and total mass flow rate are variable. Uniform cell widths are maintained across the structure because graded cell widths appear to have relatively small effects on satisfying the objectives for these boundary conditions. Gradient-based solution algorithms, such as sequential quadratic programming, are employed in this phase because all variables are continuous.
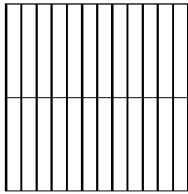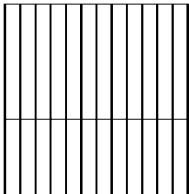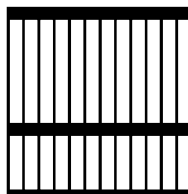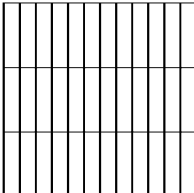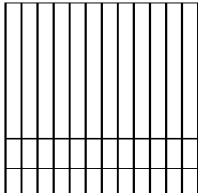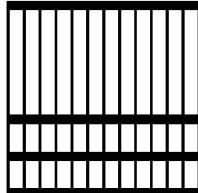
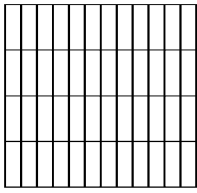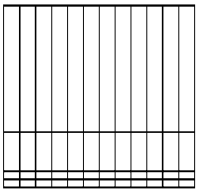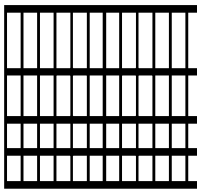|	**Uniform**	**Graded**	**Multi-objective**
12x2	**A** Cell Height: 12.28 mm Cell Width: 1.77 mm Wall Thickness-x: 0.29 mm Wall Thickness-y: 0.15 mm $\tilde{E}_x / E_s$: 0.02 $\tilde{E}_y / E_s$: 0.15 Q_{total}: 110.38 W	**B** Cell Height: 14.78, 9.77 mm Cell Width: 1.77 mm Wall Thickness-x: 0.29 mm Wall Thickness-y: 0.15 mm $\tilde{E}_x / E_s$: 0.02 $\tilde{E}_y / E_s$: 0.15 Q_{total}: 110.44 W	**C** Cell Height: 13.65, 7.01 mm Cell Width: 1.72 mm Wall Thickness-x: 0.34 mm Wall Thickness-y: 1.45 mm $\tilde{E}_x / E_s$:0.17 $\tilde{E}_y / E_s$:0.18 Q_{total}: 94.96 W
12x3	**D** Cell Height: 8.13 mm Cell Width: 1.77 mm Wall Thickness-x: 0.29 mm Wall Thickness-y: 0.15 mm $\tilde{E}_x / E_s$: 0.02 $\tilde{E}_y / E_s$: 0.15 Q_{total}: 107.05 W	**E** Cell Height: 17.26, 3.69, 3.45 mm Cell Width: 1.79 mm Wall Thickness-x: 0.27 mm Wall Thickness-y: 0.15 mm $\tilde{E}_x / E_s$: 0.02 $\tilde{E}_y / E_s$: 0.14 Q_{total}: 108.61 W	**F** Cell Height: 13.25, 3.51, 3.38 mm Cell Width: 1.67 mm Wall Thickness-x: 0.38 mm Wall Thickness-y: 1.22 mm $\tilde{E}_x / E_s$: 0.19 $\tilde{E}_y / E_s$: 0.20 Q_{total}: 88.66 W
12x4	**G** Cell Height: 6.06 mm Cell Width: 1.79 mm Wall Thickness-x: 0.27 mm Wall Thickness-y: 0.15 mm $\tilde{E}_x / E_s$: 0.03 $\tilde{E}_y / E_s$: 0.14 Q_{total}: 104.38 W	**H** Cell Height: 16.97, 5.08, 0.85, 0.85 Cell Width: 1.92 mm Wall Thickness-x: 0.25 mm Wall Thickness-y: 0.15 mm $\tilde{E}_x / E_s$: 0.03 $\tilde{E}_y / E_s$: 0.13 Q_{total}: 106.44 W	**I** Cell Height: 7.61, 5.53, 3.42, 3.47 Cell Width: 1.69 mm Wall Thickness-x: 0.36 mm Wall Thickness-y: 0.99 mm $\tilde{E}_x / E_s$: 0.20 $\tilde{E}_y / E_s$: 0.19 Q_{total}: 84.91 W

Fig. 11   Uniform, functionally graded, and multiobjective LCA heat exchanger cross sections.

It is possible to combine phases 1 and 2 in this case and to solve the resulting mixed discrete/continuous design problems with approaches such as genetic algorithms. However, a single-stage approach may not be pragmatic for a more general case in which distinct cell topologies are identified or generated (with topology design techniques) as preliminary concepts and subsequently refined for multifunctional performance. Thus, we have chosen to separate the synthesis into two distinct phases for simplicity of solution, clarity of description, and agreement with the generally valid two-phase approach advocated in this section.

Design phase 2 can be separated into two parts or stages, as indicated in Table 2. In phase 2a, designs are synthesized that maximize exclusively the total rate of steady-state heat transfer because this is the most important design objective in this example. In phase 2b, multifunctional designs are explored by the inclusion of elastic stiffness objectives as well.

The outcome of phase 2a is a set of graded LCA designs that maximize heat transfer for each of the promising cell configurations identified in phase 1. The resulting designs are shown in Figs. 11b,

11e, and 11h. As shown in Fig. 11, cells at the top of the structure (near the heat source where cell wall temperatures are higher) tend to elongate to facilitate heat transfer. Cell walls tend to be thin for both periodic and graded designs because the solid material is high-conductivity copper. The overall structural elastic stiffness in the x direction is especially low for these designs due to thin, sparse horizontal cell walls. A slight improvement in total heat transfer is realized by grading the cells. It is likely that the benefits of graded cells would be enhanced by increased temperature gradients within the structure, for example, due to a higher temperature heat source or a lower temperature, noninsulated bottom surface.

Finally, in phase 2b, graded structures are designed to maximize a combination of total heat transfer Q_{total} and overall structural elastic stiffness in the x and y directions, $\tilde{E}_x/E_s$ and $\tilde{E}_y/E_s$, respectively. This is a multiobjective design exercise in which the objective function in Fig. 8 is employed with weights of 0.5, 0.25, and 0.25 for Q_{total}, $\tilde{E}_x/E_s$, and $\tilde{E}_y/E_s$, respectively. The aim is to minimize a weighted sum of underachievements, d_i^-, for each goal, that is, a weighted sum of the normalized differences between the actual value of each performance parameter and the target value for
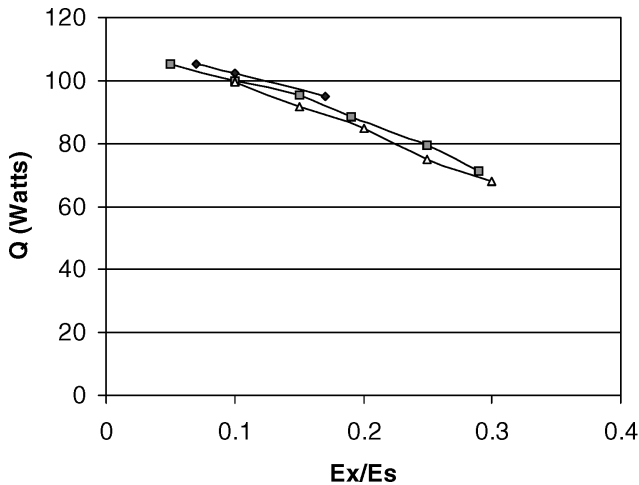
Fig. 12 Tradeoffs between total heat transfer and effective stiffness for $\blacklozenge$, 12 × 2; $\blacksquare$, 12 × 3; and $\triangle$, 12 × 4 LCA structures.

the parameter, provided that actual performance does not exceed the target value. If performance exceeds a target value, this over-achievement is not considered in the objective function. The target values for each objective, $Q_{\text{total-target}}$, $(\tilde{E}_x/E_s)_{\text{target}}$, and $(\tilde{E}_y/E_s)_{\text{target}}$, are adjusted to facilitate the exploration of a range of design capabilities. For example, by setting an ambitious target for total heat transfer rate (110 W) and achievable target values for overall structural elastic stiffness (0.05, 0.1, 0.15, 0.2, 0.25, and 0.3, expressed as fractions of the elastic modulus of solid material E_s), a family of designs are generated that exhibit a range of tradeoffs between thermal and structural performance.

Achievable tradeoffs between total heat transfer rate and overall structural elastic stiffness are illustrated in Fig. 12 for 12 × 2, 12 × 3, and 12 × 4 configurations. Sample multi-objective designs are illustrated in Figs. 11c, 11f, and 11i. In Fig. 11, it is apparent that the multiobjective designs have much thicker walls to achieve higher overall structural elastic stiffness. The multiobjective designs also have lower total heat transfer rates than the other designs. With smaller cell sizes and larger cell wall thicknesses in the multi-objective designs, a portion of the total heat transfer rate is sacrificed to achieve higher elastic stiffness. As the aspect ratio of cell wall thickness to cell dimension increases, it also becomes easier to manufacture the cells. As a rule of thumb, aspect ratios of 0.08 and above are manufacturable with current techniques. Only the multi-objective designs in Fig. 11 strictly meet this criterion. Although it is feasible to manufacture these functionally graded cellular materials with the LCA manufacturing process, note that formalisms for design of functionally graded, two-dimensional cellular materials have not been previously presented.

IV. Conclusions

A method has been developed for the design of multifunctional cellular materials. The approach is based on a multi-objective decision support model and facilitates the synthesis of a family of designs that satisfy constraints and bounds and embody a range of effective compromises among multiple, conflicting goals, such as overall structural elastic stiffness and total heat transfer rate. In the early stages of design, it is particularly important to generate such a family of concepts that represents the scope of the multifunctional design space and offers distinct alternatives for further design and analysis. The design approach itself is independent of functional domain; thus, it is possible to balance goals and requirements from alternative functional perspectives—such as acoustics, electromagnetism, or economics—in addition to or instead of heat transfer and solid mechanics.

With this design approach, functionally graded, two-dimensional cellular structures are designed with desirable structural and thermal capabilities. An efficient, flexible finite difference algorithm, coupled with the multi-objective decision support model, facilitates

efficient, accurate design of a family of multifunctional structures. Periodic, functionally graded, and multi-objective structures are designed and compared. Tradeoffs between total heat transfer rates and overall structural elastic stiffness are demonstrated. In the future, the analysis techniques that complement the design approach will be extended to accommodate a broader range of cellular topologies, variations in boundary conditions, manufacturability, and detailed modeling of the structural behavior of nonperiodic cellular structures.

We envision several innovative, high-impact applications of multifunctional honeycomb materials. For example, stiffened plate elements and multiply layups of LCAs may be designed and manufactured to meet requirements of lightweight structural stiffness, combined with internal damping characteristics achieved by polymer injection into selected cells to attenuate high-frequency vibration modes. Traditionally, either passive viscoelastic coatings or active vibration suppression methods are employed. Linear cellular materials may be designed and fabricated as structural heat exchangers that are required to resist bending and membrane forces as structural members while transferring heat away from high heat flux regions, thereby combining functions normally met by structural elements with separate heat exchangers. Structural elements in satellites or wings in hypersonic aircraft may be actively cooled to provide thermal management associated with solar radiation heat flux or supersonic aerodynamic heat generation, respectively.

References

[1]Evans, A. G., Hutchinson, J. W., Fleck, N. A., Ashby, M. F., and Wadley, H. N. G., "The Topological Design of Multifunctional Cellular Materials," *Progress in Materials Science*, Vol. 46, No. 3-4, 2001, pp. 309–327.

[2]Hayes, A. M., Wang, A., Dempsey, B. M., and McDowell, D. L., "Mechanics of Linear Cellular Alloys," *Proceedings of IMECE 2001, International Mechanical Engineering Congress and Exposition*, American Society of Mechanical Engineers, New York, 2001.

[3]Lu, T. J., "Heat Transfer Efficiency of Metal Honeycombs," *International Journal of Heat and Mass Transfer*, Vol. 42, No. 11, 1999, pp. 2031–2040.

[4]Cochran, J. K., Lee, K. J., McDowell, D. L., and Sanders, T. H., "Low Density Monolithic Honeycombs by Thermal Chemical Processing," *Proceedings of the 4th Conference on Aerospace Materials, Processes, and Environmental Technology*, 2000.

[5]Church, B. C., Dempsey, B. M., Clark, J. L., Sanders, T. H., and Cochran, J. K., "Copper Alloys from Oxide Reduction for High Conductivity Applications," *Proceedings of IMECE 2001, International Mechanical Engineering Congress and Exposition*, American Society of Mechanical Engineers, New York, 2001.

[6]Torquato, S., Gibiansky, L. V., Silva, M. J., and Gibson, L. J., "Effective Mechanical and Transport Properties of Cellular Solids," *International Journal of Mechanical Sciences*, Vol. 40, No. 1, 1998, pp. 71–82.

[7]Gu, S., Lu, T. J., and Evans, A. G., "On the Design of Two-Dimensional Cellular Metals for Combined Heat Dissipation and Structural Load Capacity," *International Journal of Heat and Mass Transfer*, Vol. 44, No. 11, 2001, pp. 2163–2175.

[8]Incropera, F. P., and DeWitt, D. P., *Fundamentals of Heat and Mass Transfer*, Wiley, New York, 1996.

[9]Black, W. Z., and Hartley, J. G., *Thermodynamics*, Harper and Row, New York, 1996.

[10]Roberson, J. A., and Crowe, C. T., *Engineering Fluid Mechanics*, Wiley, New York, 1997.

[11]Faires, J. D., and Burden, R., *Numerical Methods*, Brooks/Cole, Pacific Grove, CA, 1998.

[12]George, A., "Direct Solution of Sparse Positive Definite Systems: Some Basic Ideas and Open Problems," *Sparse Matrices and Their Uses*, edited by I. S. Duff, Academic Press, London, 1981, pp. 283–306.

[13]Barrett, R., Berry, M., Chan, T. F., Demmel, J., Donato, J. M., Dongarra, J., Eijkhout, V., Pozo, R., Romine, C., and Van der Horst, H., *Templates for the Solution of Linear Systems: Building Blocks for Iterative Methods*, Society for Industrial and Applied Mathematics, Philadelphia, PA, 1994.

[14]Dempsey, B. M., "Thermal Properties of Linear Cellular Alloys," M.S. Thesis, G. W. Woodruff School of Mechanical Engineering, Georgia Inst. of Technology, Atlanta, GA, April 2002.

[15]Oosthuizen, P. H., and Naylor, D., *An Introduction to Convective Heat Transfer Analysis*, McGraw–Hill, New York, 1999.

[16]*FLUENT*, ver. 6.0, Fluent, Inc., Lebanon, NH, 1998.

[17]Gibson, L. J., and Ashby, M. F., *Cellular Solids: Structure and Properties*, Cambridge Univ. Press, Cambridge, England, U.K., 1997.

[18]Mistree, F., Hughes, O. F., and Bras, B. A., "The Compromise Decision Support Problem and the Adaptive Linear Programming Algorithm," *Structural Optimization: Status and Promise*, edited by M. P. Kamat, AIAA, Washington, DC, 1993, pp. 247–286.

[19]Marston, M., Allen, J. K., and Mistree, F., "The Decision Support Problem Technique: Integrating Descriptive and Normative Approaches in Decision Based Design," *Journal of Engineering Valuation and Cost Analysis*, Vol. 3, No. 2, 2000, pp. 107–129.

[20]*iSIGHT*, ver. 6.0, Engineous Software, Inc., Cary, NC, 2001.

B. Sankar
Associate Editor